



**HAL**  
open science

## Dynamic response of viscoelastic multiple-core sandwich structures

M. D'ottavio, A. Krasnobrizha, E. Valot, O. Polit, R. Vescovini, L. Dozio

### ► To cite this version:

M. D'ottavio, A. Krasnobrizha, E. Valot, O. Polit, R. Vescovini, et al.. Dynamic response of viscoelastic multiple-core sandwich structures. *Journal of Sound and Vibration*, 2021, 491, pp.115753 -. 10.1016/j.jsv.2020.115753 . hal-03493776

**HAL Id: hal-03493776**

**<https://hal.science/hal-03493776v1>**

Submitted on 21 Nov 2022

**HAL** is a multi-disciplinary open access archive for the deposit and dissemination of scientific research documents, whether they are published or not. The documents may come from teaching and research institutions in France or abroad, or from public or private research centers.

L'archive ouverte pluridisciplinaire **HAL**, est destinée au dépôt et à la diffusion de documents scientifiques de niveau recherche, publiés ou non, émanant des établissements d'enseignement et de recherche français ou étrangers, des laboratoires publics ou privés.



Distributed under a Creative Commons Attribution - NonCommercial 4.0 International License

# Dynamic response of viscoelastic multiple-core sandwich structures

M. D'Ottavio<sup>a,1</sup>, A. Krasnobrizha<sup>a</sup>, E. Valot<sup>a</sup>, O. Polit<sup>a</sup>, R. Vescovini<sup>b</sup>, L. Dozio<sup>b</sup>

<sup>a</sup>*Laboratoire Energétique Mécanique Electromagnétisme, Université Paris Nanterre  
50, rue de Sèvres, 92410 Ville d'Avray, France*

<sup>b</sup>*Dipartimento di Scienze e Tecnologie Aerospaziali, Politecnico di Milano  
Via La Masa 34, 20156 Milano, Italy*

---

## Abstract

This work focuses on the free and forced vibrations of sandwich beams and plates hosting an arbitrary number of damping cores. A fractional derivatives Zener-type model is adopted for representing the frequency-dependent viscoelastic behaviour, along with conventional series developments. The structural models are formulated within an established variable kinematics approach, which enables to investigate the role of specific assumptions and to identify the most accurate model at a least number of degrees of freedom. Approximate solutions are found by a computationally efficient Ritz method that allows to take into account any type of boundary conditions. Modal loss factors and damped eigenfrequencies are obtained from a complex eigenvalue problem, for which a modal strain energy approach or a complex eigensolution can be employed. Frequency responses can be computed by a direct approach or by elementary modal projection algorithms. Results are reported for conventional and innovative sandwich configurations. Different modelling and solution strategies are compared and the role of transverse normal deformation of the mechanically weak viscoelastic plies is particularly emphasised.

*Keywords:* Viscoelastic damping, Variable kinematics, Ritz method, Fractional derivatives model, Multiple-core sandwich

---

## 1. Introduction

Viscoelastic materials (VEM) have been proven to be an attractive means for improving structural vibration damping, which is of particular relevance for noise attenuation [1] but also for enhancing dynamic stability, impact resistance and fatigue life. These materials are particularly effective when implemented as constrained layers, a configuration that can be realised within either

---

<sup>1</sup>Corresponding author. Dr.-Ing. Michele D'Ottavio, Email: mdottavi@parisnanterre.fr

6 passive or hybrid vibration control approaches [2]. In order to properly account for the damping  
7 performances in the design phase, appropriate modelling techniques are required. The inherent  
8 complexity of both, the underlying physical mechanisms characterising the viscoelastic behaviour  
9 and the resulting structural response, has stimulated an important research effort. In the follow-  
10 ing, attention is restricted to linear and non-ageing VEM in an isothermal setting, although it is  
11 worth recalling that the operating temperature is an important parameter of the viscoelastic damp-  
12 ing properties [3]. Furthermore, since the present work is focused on the harmonic response, i.e.,  
13 free-vibration and frequency response, the attention will be mainly given to structural models in-  
14 scribed within the conventional Complex Modulus Approach (CMA).

15 The frequency-dependent dynamic modulus and loss factor of the most employed VEM, such as  
16 elastomers, has been of main concern. The Golla-Hughes-McTavish (GHM) [4] and the Anelastic  
17 Displacement Field (ADF) [5] approaches introduce internal variables for describing the viscoelas-  
18 tic behaviour in terms of generalised rheological models, which represent the dissipation function as  
19 a sum of individual relaxation processes, such as the generalised Maxwell or Kelvin-Voigt models.  
20 These integral approaches are quite compatible with the conventional Finite Element (FE) discreti-  
21 sation of the equation of motion in time domain, but can also be employed in the frequency domain  
22 within the CMA. However, an accurate representation of weakly frequency-dependent materials re-  
23 quires a large number of parameters. A convenient representation of this class of materials relies on  
24 a constitutive law described by fractional derivatives (FD) [6–8], an approach that has several ap-  
25 pealing features as it is causal, mechanically justified and thermodynamically sound, and it allows  
26 to describe the material behaviour over a broad frequency range with a relatively small number of  
27 parameters, typically four or five [9, 10]. Despite the evaluation of differential operators of frac-  
28 tional order comes along with a certain computational burden [11], the use of FD models in the  
29 frequency domain within the CMA is straightforward.

30 From the computational point of view, the determination of modal loss factors and damped  
31 eigenmodes of structures with embedded frequency-dependent materials amounts to solve complex  
32 and nonlinear eigenvalue problems. Several numerical techniques have been devised for an efficient  
33 though accurate solution of this challenging algebraic problem: the nonlinear Arnoldi method [12],  
34 the Order-Reduction-Iteration approach [13], or methods based on an asymptotic expansion of the  
35 eigensolution [14, 15]. The so-called Direct Frequency Response (DFR) can be alternatively used,  
36 from which the structural damping can be extracted from the resonant peaks [16]. The Modal Strain

37 Energy (MSE) approach reduces the computational cost of the complex eigenvalue problem by us-  
38 ing the undamped mode shapes for estimating the energy contribution of the viscoelastic damping  
39 and thus the loss factors [17, 18]. This approximation appears particularly meaningful for lightly  
40 damped structures in which the damped modes differ only marginally from the undamped ones.  
41 An Iterative MSE (IMSE) scheme allows to extend the MSE approach to frequency-dependent vis-  
42 coelasticity [19, 20]. Several algorithms improve the accuracy of the MSE approach upon retaining  
43 the imaginary part of the eigenmodes, see, e.g., [2]. A comprehensive numerical assessment of  
44 modal projection algorithms can be found in [21].

45 From the structural point of view, the constrained layer configuration is a sandwich construction,  
46 in which the VEM layer acts as the soft core placed amid the basis structure and a stiff constraining  
47 layer. In such a configuration, the flexural vibrations of the basis structure induce a transverse shear  
48 strain of the viscoelastic material, which in turn drives a broadband energy dissipation [22, 23]. A  
49 large variety of modelling approaches have been proposed for predicting the dynamic response of  
50 these structures at a less effort, either in terms of analytical treatments or of computational cost.  
51 This aspect is of particular relevance in the framework of optimisation studies and by keeping in  
52 mind the inherent nonlinearity of frequency-dependent viscoelasticity.

53 Within classical FE discretisation techniques, the elastic skins are usually discretised using  
54 structural elements (beam/plate/shell), while solid elements are used for the VEM layer [24]. In  
55 order to reduce the modelling and computational burden associated with the use of solid elements  
56 for thin VEM layers, Rouleau *et al.* have developed viscoelastic interface elements that can be con-  
57 nected with standard solid elements available in commercial FE packages [25], while Kpeky *et*  
58 *al.* proposed models entirely based on solid-shell elements [26].

59 Many *ad-hoc* structural models have been proposed in the framework of dedicated analytical  
60 or numerical developments and the following literature review has not the aim of being exhaustive.  
61 Three different modelling approaches can be distinguished for multilayered composite structures  
62 as Equivalent Single Layer (ESL), Layer-Wise (LW), and ZigZag approaches [27–29]. In an ESL  
63 approach, the whole composite stack is homogenised and its behaviour described by a number of  
64 unknowns that is independent of the number of physical plies, whereas in a LW approach, each ply  
65 is described by a dedicated set of unknown functions. Pertain to the ESL models the well known  
66 Classical Lamination Theory (CLT), which relies on Kirchhoff-Love assumptions and neglects the  
67 transverse shear deformation, and the First-order Shear Deformation Theory (FSDT), which relies

68 on Reissner-Mindlin assumptions and retains a transverse shear deformation that is constant across  
69 the thickness. Refinements of these classical models can be classified as High-order Shear Deforma-  
70 tion Theories (HSDT) and High-order Shear and Normal Deformation Theories (HSNDT); theories  
71 pertaining to this latter group retain the transverse normal stress and employ the full 3D constitutive  
72 law. A ZigZag model can be constructed starting from a LW model and making the number of  
73 unknowns independent from the number of plies through the enforcement of physically meaningful  
74 conditions at the interfaces, i.e., the interlaminar  $C^0$ -continuity of the displacement and transverse  
75 stress fields, see, e.g., the comprehensive overview [30] and the general procedure developed in  
76 [31]. Alternatively, so-called ZigZag-Functions can be simply superposed to an ESL displacement  
77 field [32]. When dealing with sandwich structures, an ESL approach is known to be inaccurate  
78 because it is not capable to account for the strong mismatch between the stiff skins and the soft core  
79 [33, 34]. Therefore, various LW and ZigZag models have been proposed for viscoelastic sandwich  
80 structures, as discussed in the following.

81 Within a LW description, the simplest models rely on the fundamental assumption of a “weak”  
82 core that does not carry any axial stress and simply transfers the bending stresses of the stiff skins  
83 by means of a uniform transverse shear stress [22, 35–39]. However, the most frequently used  
84 models nowadays include the axial stresses in the core and the bending stiffness of the skins, i.e.,  
85 by adopting CLT for the skins and FSDT for the core, see, e.g., [40–46]. Cupiał and Nizoł proposed  
86 a critical evaluation of the simplifying assumption of nil transverse shear stress in the elastic skins  
87 [47]. Examples of LW models employing FSDT for all layers, elastic and VEM, can be found in  
88 [48–50]. In order to improve the transverse shear strain that drives the viscoelastic damping, HSDT  
89 have been used for the VEM layer, see e.g., [51–53]. It is worth highlighting that, according to [53],  
90 enforcing the interlaminar continuity of the transverse shear stresses does not substantially improve  
91 the vibration response of the viscoelastic sandwich.

92 In order to reduce the number of degrees of freedom (dof) with respect to LW approaches,  
93 ZigZag models for sandwich structures with VEM cores have been proposed, e.g., in [54–57] for  
94 beams and in [58] for plates.

95 All the aforementioned models discard the transverse normal strain energy contribution, which,  
96 however, can contribute substantially to the viscoelastic energy dissipation depending on the vibra-  
97 tion mode of the structure [23]. A more limited number of works consider the so-called transverse  
98 compressional damping along with the transverse shear damping, see, e.g., [59, 60]. Ref. [60] is

99 of particular relevance as it employs a LW description for the sandwich structure, in which CLT is  
100 used for modelling the skins and variable kinematics can be adopted for the VEM core by referring  
101 to polynomial expansions of different orders for the in-plane and transverse displacements. Vari-  
102 able kinematics approaches are very useful for assessing the accuracy of different models, which is  
103 known to be highly problem-dependent [61].

104 The most established variable kinematics approach has been systematically developed by Car-  
105 rera [62]. By virtue of a compact index notation, the so-called Carrera Unified Formulation (CUF)  
106 enables the implementation in a unique software of structural models ranging from the most con-  
107 strained CLT and FSDT up to quasi-3D models, including ESL, LW as well as ZigZag models based  
108 on HSDT or HSNDT and MZZF. CUF has been formally generalised to allow different expansion  
109 orders and descriptions to be used for individual displacement components (Generalized Unified  
110 Formulation, GUF) [63] as well as for groups of plies, the *sublaminates* (Sublaminated Generalized  
111 Unified Formulation, SGUF) [64]. The application of CUF to composite structures including VEM  
112 layers can be found in [65–69].

113 This paper presents for the first time the extension of the SGUF approach to composite sandwich  
114 with frequency-dependent VEM layers. The partial differential equations associated to the variable  
115 kinematics plate models are solved in weak form by a highly efficient Ritz method [70]. The SGUF-  
116 Ritz approach has already demonstrated its versatility and accuracy in the static, free-vibration and  
117 stability analysis of sandwich plates and shells [71–74]. In particular, the present Ritz solution  
118 has proven to converge rapidly even in presence of highly anisotropic structures and is capable of  
119 handling any type of boundary conditions [75].

## 120 2. Viscoelastic models in CMA

121 The time-dependent constitutive law of a viscoelastic material (VEM) is expressed in the fre-  
122 quency domain through a Fourier transform, which yields the following definition of a complex  
123 modulus:

$$E^*(i\omega) = E'(\omega) + i E''(\omega) = E'(\omega) [1 + i \eta(\omega)] \quad (1)$$

124 Throughout the paper, complex variables are denoted by an asterisk and  $i = \sqrt{-1}$  is the imaginary  
125 unit. In Eq. (1),  $E'$  is the dynamic or storage modulus and  $E''$  is the loss modulus. The ratio between

126 the loss and storage modulus measures the material damping through the loss factor  $\eta$  :

$$\eta(\omega) = \frac{E''(\omega)}{E'(\omega)} \quad (2)$$

### 127 2.1. Anelastic Displacement Fields model

128 Following Lesieutre and Bianchini [5], a frequency-dependent viscoelastic material can be de-  
129 scribed within the CMA as a series of  $j = 1, 2 \dots n$  Kelvin-Voigt elements and an elastic spring  
130 according to the following expression:

$$G^*(\omega) = G_0 \left( 1 + \sum_{j=1}^n \frac{\Delta_j \omega}{\omega - i \Omega_j} \right) \quad (3)$$

131 where  $G_0 = G^*(\omega \rightarrow 0)$  is the “relaxed” or static modulus of elasticity, and  $1/\Omega_j$  and  $\Delta_j$  are the  
132 relaxation time and strength, respectively, of the  $j^{\text{th}}$  Kelvin-Voigt element. At very high frequencies,  
133 the VEM response is purely elastic and is characterised by the high-frequency limit of the dynamic  
134 modulus (“unrelaxed” modulus)  $G_\infty = G^*(\omega \rightarrow \infty) = G_0(1 + \sum_j \Delta_j)$ .

### 135 2.2. Fractional derivatives Zener model

136 The fractional derivatives Zener (FDZ) model employed in this work describes the VEM be-  
137 haviour in the frequency domain by means of the following expression that involves only 4 param-  
138 eters [9]

$$G^*(\omega) = \frac{G_0 + G_\infty (i \omega \tau)^\alpha}{1 + (i \omega \tau)^\alpha} \quad (4)$$

139 As in Eq. (3),  $G_0$  is the static modulus and  $G_\infty = G^*(\omega \rightarrow \infty)$  is the unrelaxed modulus, while  $\alpha$  is  
140 the fractional order of derivatives and  $\tau$  the relaxation time. In order to respect the second principle  
141 of thermodynamics, the following conditions must hold [8]:

$$G_\infty > G_0 > 0, \quad \tau > 0, \quad \text{and} \quad 0 < \alpha \leq 1 \quad (5)$$

### 142 2.3. Identification of viscoelastic material parameters

143 A procedure is described in the following, which allows to identify the FDZ model parameters  
144 characterising the frequency-dependent behaviour of a VEM. In particular, the procedure is applied  
145 to 2 materials with different data sources, namely the 3M ISD112 polymer, that has been often  
146 described in terms of ADF series expansions [5, 19], and the Deltane 350, for which FDZ models  
147 have been identified from an experimental master curve [76, 77].

148 Starting from a reference curve describing the frequency-dependent complex modulus, which  
149 may be defined by an ADF model or from other experimentally collected data, the parameters of the  
150 FDZ model are determined employing an inverse optimisation procedure whose objective function  
151 is the mean square error of the storage and loss moduli  $G'$  and  $G''$  over the considered frequency  
152 range. A 4-dimensional optimisation problem is thus formulated, whose unknown parameters are  
153  $G_0, G_\infty, \tau$  and  $\alpha$  under the constraints given in Eq. (5). It is noticed that the static and unrelaxed  
154 moduli  $G_0$  and  $G_\infty$  can be uniquely determined within a least-square method once the parameters  $\alpha$   
155 and  $\tau$  are fixed. Several optimisation algorithms have been investigated for the identification, and  
156 it has been found that the meta-heuristic Particle Swarm Optimisation (PSO) method [78] provided  
157 the most accurate results in a robust manner, taking into account the very different orders of magni-  
158 tude of the involved parameters and the slightly oscillating nature of the globally convex objective  
159 function. A population of 10 particles are employed to solve the problem, which is considered to be  
160 converged when the tolerance value of  $10^{-6}$  is reached for the objective function for 10 consecutive  
161 iterations. For the applications discussed in this paper, convergence could be generally achieved  
162 within a maximum of 70 iterations.

163 For the 3M ISD112 at 27°C, Lesieutre and Bianchini provided an experimental identification of  
164 the ADF parameters related to a series expansion involving  $n = 1, 3$  and 5 Kelvin-Voigt elements  
165 [5]. The description given by Eq. (3) with  $n = 5$  was shown to very well match the experimental  
166 response over the frequency range 8 – 8000 Hz. An ADF model with  $n = 3$  has been independently  
167 identified over the frequency range 20 – 5000 Hz by Trindade *et al.* [19]. The present identification  
168 of the FDZ parameters is carried out starting from the ADF models in [5] with  $n = 5$  (ADF-5) and  
169 with  $n = 3$  (ADF-3). The objective function is defined for both cases over two different frequency  
170 ranges, namely the FR1 8 – 8000 Hz and the FR2 20 – 5000 Hz. The relaxed modulus  $G_0$  has the  
171 same meaning in the FDZ and ADF models and has been here considered as a fixed value, which  
172 reduces the optimisation problem to a 3-dimensional one. It has been found that more accurate  
173 optimisation results could be obtained by letting  $G_\infty$  free to be identified concurrently with  $\alpha$  and  $\tau$ .  
174 The numerical values for the FDZ model parameters obtained from the identification are reported  
175 in Tab. 1. The corresponding frequency-dependent storage modulus and loss factor are given in  
176 Fig. 1 for the ADF-5 and ADF-3 case. The FDZ models identified from the ADF-5 over the two  
177 frequency ranges provide very similar, smooth curves that fit well the reference. Also the FDZ  
178 models obtained from the ADF-3 model yield smooth curves, however, some discrepancies are



Model	Freq. range	$G_0$ [MPa]	$G_\infty$ [MPa]	$\tau$ [ $\mu$ s]	$\alpha$
ADF-5	FR1	0.462	152.76	0.522	0.675
	FR2	0.462	171.39	0.444	0.675
ADF-3	FR1	0.493	150.70	0.646	0.691
	FR2	0.493	180.96	0.356	0.674

Table 1: ISD112 at 27°C: FDZ model parameters identified from the ADF models of [5] with  $n = 5$  and  $n = 3$ .

179 visible in particular for the loss factor due to the slightly oscillating behaviour displayed by the  
180 ADF model. Moreover, the curves obtained over the two frequency ranges FR1 and FR2 differ in  
181 a more visible manner from each other compared to the curves identified starting from the ADF-5  
182 model.

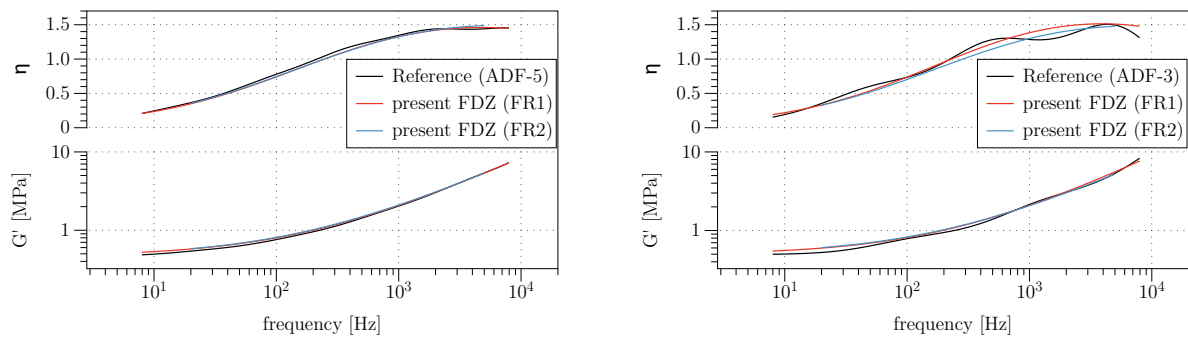


Figure 1: Frequency-dependent storage modulus and loss factor for ISD112: Reference [5] and FDZ curves identified over the frequency ranges FR1 and FR2 from ADF-5 model (left) and ADF-3 model (right).

183 For the Deltane 350, the identification is carried out starting from the master curve at 12°C  
184 reported in [76]. In this case, all four FDZ material parameters are optimised, 40 particles are thus  
185 used in the PSO algorithm. Table 2 lists the FDZ parameters obtained by the present identification  
186 along with 3 different sets reported in [76, 77]: the set “FDZ-anlt”, whose parameters have been  
187 analytically estimated by Rouleau [76] according to [11], and the two sets “FDZ-exp1” and “FDZ-  
188 exp2” identified from the experimental master curve [76, 77]. The frequency-dependent storage  
189 modulus and loss factor of the resulting 4 FDZ models are graphically compared in Fig. 2, in  
190 which the reference curve obtained upon digitalisation of the master curve of the manufacturer is  
191 also given. One can notice that the analytical estimate of the FDZ parameters may yield to rather  
192 inaccurate results, while a reasonable agreement is found for the present FDZ and the FDZ-exp2

Model	$G_0$ [MPa]	$G_\infty$ [GPa]	$\tau$ [ $\mu$ s]	$\alpha$
FDZ-anlt [76]	1.40	0.54	0.52	0.59
FDZ-exp1 [76]	1.60	0.37	0.69	0.63
FDZ-exp2 [77]	1.88	0.78	0.15	0.50
Present	1.90	0.37	0.56	0.51

Table 2: FDZ model parameters for Deltane 350 at 12°C.

193 models, whose parameters are identified directly from the experimental curves.

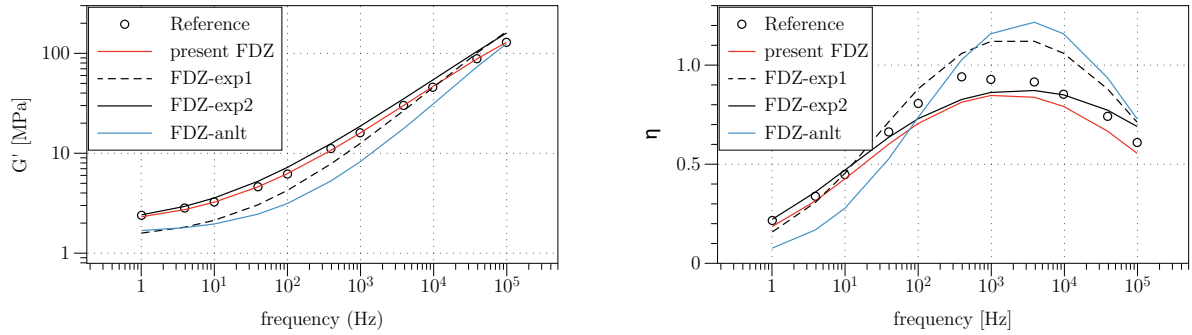


Figure 2: Frequency-dependent storage modulus (left) and loss factor (right) for Deltane 350: Reference curves and FDZ models.

### 194 3. Derivation of the governing equations

#### 195 3.1. Description of the geometry

196 Let a composite plate occupy the volume  $V = \Omega \times \left[-\frac{h}{2} \leq x_3 \leq \frac{h}{2}\right]$ , with  $h$  denoting the uniform  
197 thickness and  $\Omega = [0, L_1] \times [0, L_2]$  the reference surface on the  $(x_1, x_2)$ -plane. Let further be the  
198 plate composed of  $p = 1, 2, \dots, N_p$  perfectly bonded and homogeneous plies, each of thickness  
199  $h_p$ , stacked along the thickness direction  $x_3 \equiv z$ . As illustrated in Fig. 3, the SGUF approach  
200 relies on the subdivision of the composite stack into  $k = 1, 2, \dots, N_k$  sublaminates, each of uniform  
201 thickness  $h_k$  and composed of  $N_p^k$  adjacent plies. In the following, quantities related to the ply  $p$   
202 of the sublaminate  $k$  will be indicated by  $(\cdot)^{p,k}$ ,  $p$  indicating the ply index and  $k$  the sublaminate  
203 index. Ply- and sublaminate-specific coordinates are introduced as  $z_p \in \left[-\frac{h_p}{2}, \frac{h_p}{2}\right]$  and  $z_k \in \left[-\frac{h_k}{2}, \frac{h_k}{2}\right]$ ,  
204 respectively. The following dimensionless coordinates are thus defined as

$$\zeta_p = \frac{2z_p}{h_p}; \quad \zeta_k = \frac{2z_k}{h_k} \quad (6a)$$

205 where the following relation holds

$$\zeta_p = \frac{h_k}{h_p} \zeta_k + \frac{2}{h_p} (z_{0k} - z_{0p}) \quad (6b)$$

206 with  $z_{0p}$  and  $z_{0k}$  denoting the coordinates of the midplanes of the ply and sublaminate, respectively.

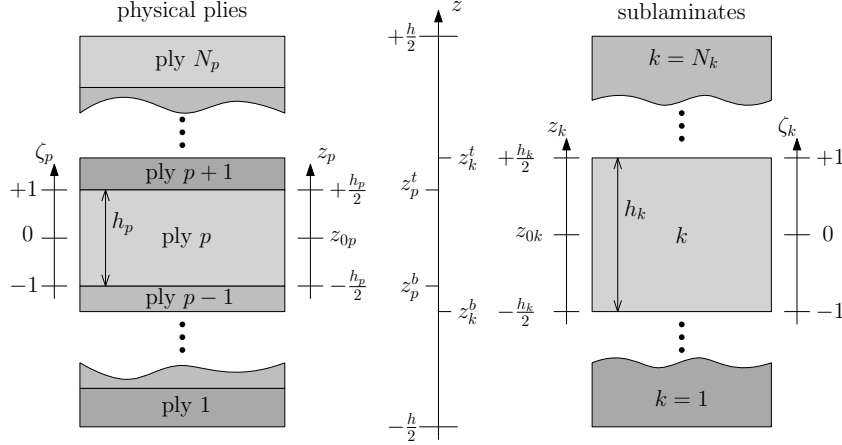


Figure 3: SGUF: geometry description and employed coordinates across the thickness.

### 207 3.2. Variable kinematics plate models in SGUF

208 The governing equations of displacement-based plate models shall be obtained upon introducing  
 209 in axiomatic sense the through-the-thickness approximation for the kinematic field  $u_i(x_\alpha, z)$  into the  
 210 equilibrium statement in weak form. For a dynamic system, reference is conveniently made to  
 211 Hamilton's principle and to the resulting expression:

$$\int_V \delta \epsilon_{ij} \sigma_{ij} + \delta u_i \rho \ddot{u}_i \, dV = \int_{S_t} \delta u_i \bar{t}_i \, dS \quad (7)$$

212 Tensor notation as well as summation convention over repeated indexes is adopted, with Latin  
 213 indexes taking values in the set  $\{1, 2, 3\}$ . In Eq. (7),  $\epsilon_{ij}$  and  $\sigma_{ij}$  represent the strain and stress tensors,  
 214 respectively,  $\rho$  is the mass density,  $\delta$  denotes an admissible virtual variation, and  $\bar{t}_i$  is the external  
 215 traction imposed at boundary region  $S_t$ . For the sake of simplicity, let  $S_t = \Omega \times \pm \frac{h}{2}$ , i.e., the top and  
 216 bottom surfaces of the plate. Introducing the subdivision into sublaminates and upon separating the  
 217 integrals over the surface  $\Omega$  and the thickness  $h$ , the variational statement Eq. (7) reads

$$\sum_{k=1}^{N_k} \sum_{p=1}^{N_p^k} \int_\Omega \int_{h_p} \delta \epsilon_{ij}^{p,k} \sigma_{ij}^{p,k} + \delta u_i^{p,k} \rho^{p,k} \ddot{u}_i^{p,k} \, dz \, dx_1 \, dx_2 = \int_\Omega \delta u_i \bar{t}_i |_{z=\pm \frac{h}{2}} \, dx_1 \, dx_2 \quad (8)$$

218 Note that Greek indexes are taken to range in  $\{1, 2\}$ . Limiting the scope of the proposed model  
 219 within the small perturbation assumptions, the linear geometric and constitutive equations are used  
 220 to define the strains and the stress, respectively, according to

$$\epsilon_{ij}^{p,k} = \frac{1}{2} (u_{i,j}^{p,k} + u_{j,i}^{p,k}); \quad \sigma_{ij}^{p,k} = \tilde{C}_{ijlm}^{p,k} \epsilon_{lm}^{p,k} \quad (9)$$

221 where  $(\cdot)_{,i}$  denotes partial derivative with respect to  $x_i$ . The stiffness coefficients  $\tilde{C}_{ijklm}$  are allowed to  
 222 depend on the circular frequency  $\omega$  according to the viscoelastic law introduced in Section 2.

223 Variable kinematics models are next expressed by taking advantage of the compact index nota-  
 224 tion that is characteristic of Unified Formulations. SGUF models are constructed as a LW assembly  
 225 of GUF models defined in each sublaminar in terms of a polynomial expansion: the distribution  
 226 of the displacement components  $u_r^{p,k}$  ( $r = 1, 2, 3$ ) across the thickness of the  $p^{\text{th}}$  ply within the  
 227  $k^{\text{th}}$  sublaminar is postulated according to

$$u_r^{p,k}(x_1, x_2, z_p; t) = \sum_{\alpha_{u_r}=0}^{N_{u_r}^k} F_{\alpha_{u_r}}(z_p) \hat{u}_{\alpha_{u_r}}^{p,k}(x_1, x_2; t) \quad (10)$$

228 The ply-wise distributions of each individual displacement component  $u_r$ , defined by the thickness  
 229 functions  $F_{\alpha_{u_r}}(z_p)$ , are assembled to form the sublaminar distribution according to either an ESL or  
 230 an LW description. It is worth emphasising that, irrespective of the ESL or LW description adopted  
 231 for the  $k^{\text{th}}$  sublaminar, the order of the polynomial expansion  $N_{u_r}^k$  is unique for all the  $N_p^k$  plies and  
 232 it can take different values depending on the displacement component. A constant approximation  
 233 is introduced for the  $u_r^{p,k}$  variable by setting  $N_{u_r}^k = 0$  and  $F_{\alpha_{u_r}} = 1$ . The thickness functions used  
 234 for defining a linear approximation ( $N_{u_r}^k = 1$ ) are standard linear Lagrange polynomials, which in-  
 235 terpolate the values at the top and bottom of the ply (in a LW description) or of the sublaminar (in  
 236 an ESL description); this allows to enforce the perfect bond condition of adjacent plies and sub-  
 237 laminates through a straight-forward assembly procedure. Higher-order approximations are defined  
 238 upon superposing to the linear Lagrange contributions a hierarchic enrichment defined in terms of  
 239 orthogonal Legendre polynomials. Finally, an opportunely modified form of Murakami's ZigZag  
 240 Function (MZZF), which vanishes at the interfaces  $z_k = \left\{-\frac{h_k}{2}, \frac{h_k}{2}\right\}$ , can be included within an ESL  
 241 description, see also [73] for more details.

242 *3.3. Ritz approximation*

243 The trial solution for the displacement field along the in-plane coordinates  $x_\alpha$  is expressed fol-  
244 lowing a Ritz-type approach as

$$\hat{u}_{r\alpha_r}^{p,k}(x_1, x_2; t) = \sum_{i=1}^M N_{u_r i}(x_1, x_2) U_{r\alpha_r i}^{p,k}(t) \quad (11)$$

245 The trial functions  $N_{u_r i}(x_1, x_2)$  are linearly independent and form a complete set defining an ad-  
246 missible solution of Eq. (7): these are built by multiplying a product of 1D orthogonal Legendre  
247 polynomials with appropriate boundary functions, which assure the exact fulfilment of the essential  
248 boundary conditions [70, 75]. Denoting by  $R$  and  $S$  the expansion's order used along  $x_1$  and  $x_2$ ,  
249 respectively, the order of the resulting 2D approximation is thus  $M = RS$ . It is worth emphasising  
250 that Legendre polynomials have been shown to define Ritz functions with excellent convergence  
251 and stability properties and to yield the highest degree of sparsity of the resulting matrices [75]. It  
252 is finally noted that the trial functions  $N_{u_r i}(x_1, x_2)$  are independent of the sublaminates, and that the  
253 same order  $M$  of the Ritz expansion is used for all displacement components.

254 *3.4. The algebraic system*

255 The approximations across the thickness defined in Section 3.2 and the Ritz-type solution dis-  
256 cussed in Section 3.3 are introduced into the variational statement Eq. (7). The integrals along  
257 the thickness  $z \in [z_p^{\text{bot}}, z_p^{\text{top}}]$  of each ply ( $p$ ) are carried out and defined in the following compact  
258 notation:

$$\mathcal{I}_{(\partial)u_r(\partial)u_s}^{p\alpha_r\beta_s} = \int_{z_p^{\text{bot}}}^{z_p^{\text{top}}} F_{\alpha_r(\cdot,z)} F_{\beta_s(\cdot,z)} dz \quad (12)$$

259 where the index pairs  $(r, \alpha)$  and  $(s, \beta)$  are used for the virtual variations and the unknown functions,  
260 respectively. An analogous compact notation is employed to denote the integrals over the reference  
261 surface  $\Omega$  of the Ritz functions:

$$\mathcal{I}_{u_r u_s i j}^{deg h} = \int_{\Omega} \frac{\partial^{d+e} N_{u_r i}}{\partial x_1^d \partial x_2^e} \frac{\partial^{g+h} N_{u_s j}}{\partial x_1^g \partial x_2^h} dx_1 dx_2 \quad (d, e, g, h = 0, 1) \quad (13)$$

262 The virtual variations and the unknown functions are here addressed by the index pairs  $(r, i)$  and  
263  $(s, j)$ , respectively. These invariant expressions cover all possible occurrences of the volume inte-  
264 grals entering the governing equations of the plate model derived from Hamilton's principle. In  
265 fact, the integral expression for the equilibrium equation given in Eq. (7) can be stated in compact

266 notation in the following semi-discrete form:

$$\begin{aligned}
& \sum_{k=1}^{N_k} \sum_{p=1}^{N_p^k} \delta U_{r\alpha_{ur}i}^{p,k} \tilde{C}_{RS}^{p,k} Z_{(\partial)u_r(\partial)u_s}^{p\alpha_{ur}\beta_{us}} \mathcal{I}_{u_r u_s i j}^{degh} U_{\beta_{us}j}^{p,k}(t) \\
& + \sum_{k=1}^{N_k} \sum_{p=1}^{N_p^k} \delta U_{r\alpha_{ur}i}^{p,k} \rho^{p,k} Z_{u_r u_r}^{p\alpha_{ur}\beta_{ur}} \mathcal{I}_{u_r u_r i j}^{0000} \ddot{U}_{\beta_{ur}j}^{p,k}(t) \\
& = \delta U_{ri}^{(\text{top})} \mathcal{I}_{u_r P_r i}^{(\bar{z}_+)} P_r^{(\bar{z}_+)}(t) + \delta U_{ri}^{(\text{bot})} \mathcal{I}_{u_r P_r i}^{(\bar{z}_-)} P_r^{(\bar{z}_-)}(t) \quad (14)
\end{aligned}$$

267 The first term represents the contribution to the stiffness matrix, in which appear the possibly  
268 frequency-dependent stiffness coefficients  $\tilde{C}_{RS}^{p,k}$ , with  $R, S \in \{1, 2, \dots, 6\}$  according to Voigt's con-  
269 tracted vector notation. The second term defines the contribution to the mass matrix. The right-  
270 hand side represents the work of the external distributed load  $p_r(x_1, x_2, \bar{z}; t) = P_r^{\bar{z}}(t) f_r^{\bar{z}}(x_1, x_2)$  acting  
271 at  $\bar{z} = \{\bar{z}_+, \bar{z}_-\} = \left\{ \frac{h}{2}, -\frac{h}{2} \right\}$  along the direction  $r$  with a magnitude  $\bar{P}(t)$ . The load integral  $\mathcal{I}_{u_r P_r i}^{(\bar{z})}$  in  
272 Eq. (14) is thus defined as

$$\mathcal{I}_{u_r P_r i}^{(\bar{z})} = \int_{\Omega} F_{\alpha_{ur}}(\bar{z}) N_{u_r i}(x_1, x_2) f_r^{\bar{z}}(x_1, x_2) dx_1 dx_2 \quad (15)$$

273 The semi-discrete dynamic equilibrium equation Eq. (14) is next specialised to the case of a  
274 harmonic response under a temporal variation of loading amplitudes given by

$$P_r^{\bar{z}}(t) = P_r^{\bar{z}} e^{i\omega t} \quad (16)$$

275 Then, recalling the possibly frequency-dependent material properties of VEM, the following clas-  
276 sical algebraic form of the governing equation Eq. (7) is finally obtained

$$\left[ \mathbf{K}^*(\omega) - \omega^2 \mathbf{M} \right] \mathbf{U}^* = \mathbf{F} \quad (17)$$

277 where  $\mathbf{K}^*$  is the complex stiffness matrix,  $\mathbf{M}$  the real mass matrix,  $\mathbf{U}^*$  the complex generalised  
278 displacement vector and  $\mathbf{F}$  the real amplitude vector of the total applied loads. In absence of external  
279 loading, the following nonlinear eigenvalue problem is obtained from Eq. (17):

$$\left[ \mathbf{K}^*(\omega) - \lambda^2(\omega) \mathbf{M} \right] \mathbf{U}^* = \mathbf{0} \quad (18)$$

280 in which  $\mathbf{U}^*$  defines the complex modal shapes. The complex eigenvalues take the form [48]

$$\lambda^2 = \omega^2(1 + i\eta) \quad (19)$$

281 and define the damped eigenfrequencies  $\omega = \sqrt{\text{Re}(\lambda^2)}$  and the modal loss factor  $\eta = \frac{\text{Im}(\lambda^2)}{\text{Re}(\lambda^2)}$ .

### 282 3.5. Solution procedures

283 The SGUF-Ritz approach has been implemented in Matlab along with two solution strategies,  
284 which are basically distinguished between those treating the complex matrices and those based  
285 on the Modal Strain Energy (MSE) approach. A larger variety of solution algorithms along with  
286 a quantitative assessment of their accuracy vs computational time can be found in the paper by  
287 Rouleau *et al.* [21], which considers the solution of Eq. (17) on modal projection bases obtained  
288 from Eq. (18).

289 *Linear and nonlinear eigenvalue problems.* For frequency-independent VEM, Eq. (18) reduces to  
290 a linear and complex eigenvalue problem. This is solved either by the Complex Eigensolver (CE)  
291 available in Matlab, or by the classical MSE approach [16, 18], which considers a real eigenproblem  
292 and estimates the modal loss factor from the energy contributions defined by the associated real  
293 eigenmodes. For frequency-dependent VEM, the CE and MSE solution methods are implemented  
294 within an iterative scheme that employs a fixed-point iteration starting from an initial guess defined  
295 by the solution of the real eigenproblem given by  $\mathbf{K}(0)$ . The corresponding algorithms are given in  
296 Appendix A; the Iterative Complex Eigensolver (ICE) in Algorithm 1 and the Iterative Modal Strain  
297 Energy (IMSE) in Algorithm 2.

298 *Frequency response.* After discretising the frequency range of interest, the direct solution approach  
299 (Direct Frequency Response, DFR) consists in solving the linear system resulting from Eq. (17) at  
300 each value of the loading frequency. A modal projection approach is also proposed, in which the  
301 solution is obtained from the projection on a limited number of real eigenmodes defined by the MSE  
302 approach. The number of selected modes is the main parameter in this approach, depending on the  
303 frequency spectrum of interest. The interested reader is referred to the already mentioned paper by  
304 Rouleau *et al.* for other, more refined approaches for constructing reduced-order models [21].

## 305 4. Numerical results

306 Since the accuracy of the proposed modelling approach in the framework of elastic, undamped  
307 vibrations has been already demonstrated in [74, 75], all case studies presented in the following  
308 will be concerned with sandwich structures with embedded VEM layers. The modal loss factors of  
309 “conventional” single-core sandwich panels and for multiple-core sandwich panels are investigated  
310 in Section 4.1 and in Section 4.2, respectively. VEM with constant as well as frequency-dependent

311 loss factors are considered. Finally, Section 4.3 concerns the frequency response of a complex panel  
 312 consisting of a triple-core sandwich panel.

#### 313 4.1. Modal loss factors of sandwich plates

##### 314 4.1.1. Sandwich plate with frequency-independent viscoelastic core

315 A first case study analyses the first 100 modes of a sandwich plate with all edges free, for which  
 316 accurate numerical results were obtained by Zhang and Sainsbury by means of a conforming FEM  
 317 approach [38]. The geometry of the plate and the material data are summarised in Tab. 3. The VEM  
 318 core is an isotropic polymer with a constant, frequency-independent loss factor  $\eta_c$ . The kinematics  
 319 adopted for the sandwich plate consists of a LW assembly of models with  $\{N_{u_a}, N_{u_3}\} = \{1, 0\}$ , i.e.,  
 320 each ply is modelled as a Reissner-Mindlin plate with a unitary shear correction factor.

Geometric data		Material data:	elastic face	VEM core
Length	$L_1 = 348$ mm	Young's modulus	$E_f = 68.9$ GPa	$E_c = 2.67$ MPa
Width	$L_2 = 304.8$ mm	Poisson's ratio	$\nu_f = 0.3$	$\nu_c = 0.49$
Core thickness	$h_c = 0.254$ mm	Mass density	$\rho_f = 2740$ kg m <sup>-3</sup>	$\rho_c = 999$ kg m <sup>-3</sup>
Face thickness	$h_f = 0.762$ mm	Loss factor	$\eta_f = 0$	$\eta_c = \{0.1; 0.5; 1\}$

Table 3: Geometry and material data for the sandwich plate with frequency-independent VEM.

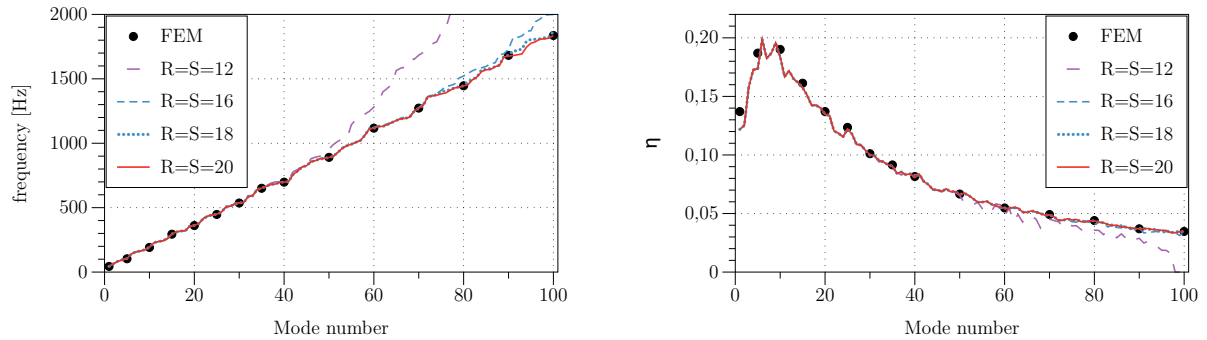


Figure 4: Modal frequencies (left) and loss factors (right) for a frequency-independent VEM with  $\eta_c = 0.5$ : convergence of present Ritz approach and comparison with FEM results by Zhang and Sainsbury [38].

321 Fig. 4 compares the eigenfrequencies and modal loss factors obtained by the present Ritz ap-  
 322 proach for the first 100 modes with those reported in [38]. These results refer to a VEM core with  
 323  $\eta_c = 0.5$  and have been obtained by the Complex Eigensolver of Matlab. The results obtained with



324 three different orders of the Ritz expansions  $R = S = \sqrt{M} = 12, 16, 20$  demonstrate the good con-  
 325 vergence of the present method. In particular, the nonuniform distribution of the modal loss factor is  
 326 well detected, with  $\eta \approx 0.2$  in the range between mode 5 and mode 10 and subsequently decreasing  
 327 with  $\eta < 0.1$  for mode higher than 30.

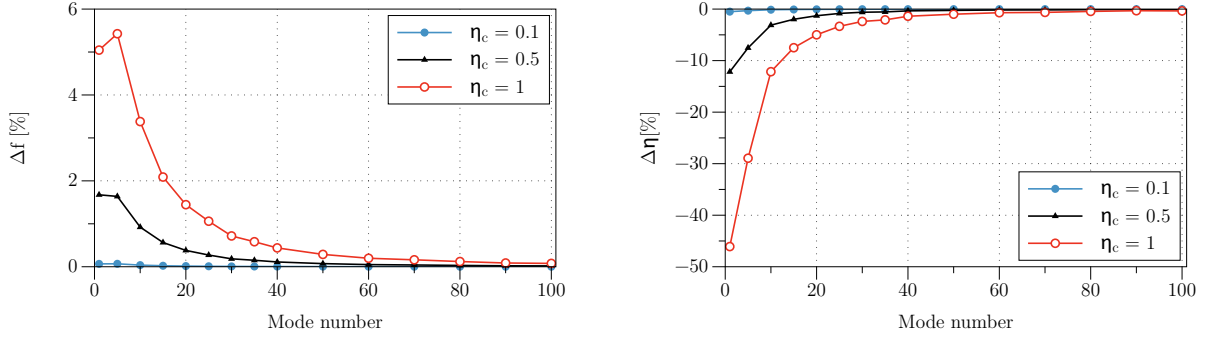


Figure 5: Percentage difference between the results of the Complex Eigensolver (CE) and the MSE approach for the eigenfrequencies (left) and modal loss factors (right) of a sandwich plate with frequency-independent VEM core.

328 This case study is also used to validate and assess the MSE approach. For this purpose, Fig. 5  
 329 reports the percentage difference of the MSE solution relative to the CE solution with respect to  
 330 modal frequencies and loss factors:  $\Delta f = \frac{f_{CE} - f_{MSE}}{f_{CE}}$  and  $\Delta \eta = \frac{\eta_{CE} - \eta_{MSE}}{\eta_{CE}}$ . The first 100 modes are  
 331 considered for VEM cores with three different material loss factors,  $\eta_c = 0.1, 0.5, 1$ . The results  
 332 show that the error introduced by the MSE approach, which disregards the complex part of the  
 333 eigenmodes, is negligibly small for  $\eta_c = 0.1$  but increases with the loss factor of the VEM. While  
 334 the discrepancy in the frequencies remains confined below 6% even for  $\eta_c = 1$ , the MSE is shown  
 335 to overestimate the loss factor of the fundamental mode by more than 40% and 10% for  $\eta_c = 1$  and  
 336  $\eta_c = 0.5$ , respectively. The error is shown to decrease with the mode number because for higher  
 337 modes the damping effect of the VEM becomes smaller. However, the accuracy of the Complex  
 338 Eigensolver comes along a quite relevant computational effort: in fact, taking as reference the time  
 339 required by the CE for solving the 100 modes, the MSE needs approximatively only half the time  
 340 to compute the same 100 modes.

#### 341 4.1.2. Sandwich plate with frequency-dependent viscoelastic core

342 This case study considers a sandwich plate whose geometry and face material are specified by  
 343 the data in Tab. 3, but whose core consists of the isotropic and frequency-dependent ISD112 VEM  
 344 ( $\rho_c = 1600 \text{ kg m}^{-3}$ ). Table 4 compares the undamped and damped eigenfrequencies and modal

345 loss factors obtained by the present approach against those given by Bilasse *et al.* [42] for 2 sets  
 346 of boundary conditions, namely a fully clamped configuration (CCCC), and a configuration with  
 347 the two edges  $x_1 = (0, L_1)$  clamped and the two other edges free (CFCF). For the VEM, Bilasse *et*  
 348 *al.* adopt the ADF-3 model as identified by Trindade *et al.* [19]. Concerning the sandwich model,  
 349 Bilasse *et al.* [42] rely on CLT for the faces and FSDT for the core. Present results are computed  
 350 employing the same 3-parameters ADF model as well as the FDZ model defined in Tab. 1 (ADF-  
 351 5, FR2). The same plate model of the previous case study is adopted, i.e., a LW kinematics with  
 352  $\{N_{u_\alpha}, N_{u_3}\} = \{1, 0\}$ . Converged Ritz solutions for the first 4 modes are obtained for all configurations  
 353 with  $R = S = 10$ . The number of parameters of the structural model is 9 and the resulting discrete  
 354 system has thus 900 DOF. The damped properties  $(f, \eta_l)$  reported in the reference work are obtained  
 355 within a “simplified approach” based on the assumption  $\omega \approx \omega_0$  [42]. Therefore, in addition to  
 356 the undamped eigenfrequency  $f_0$  and the converged values  $(f, \eta)$  obtained at the end of the iterative  
 357 procedure, Tab. 4 also reports the approximate value  $\eta_1$  that is obtained after the first iteration of the  
 358 fixed-point algorithm, see Appendix A.

BC	Mode	Ref. [42]			present ADF-3				present FDZ		
		$f_0$ [Hz]	$f$ [Hz]	$\eta_l$	$f_0$ [Hz]	$f$ [Hz]	$\eta_1$	$\eta$	$f$ [Hz]	$\eta_1$	$\eta$
CCCC	1	76.65	83.01	0.246	76.57	83.10	0.247	0.253	83.75	0.238	0.248
	2	133.54	146.61	0.258	133.49	146.91	0.259	0.269	148.15	0.261	0.274
	3	154.04	168.92	0.257	153.52	168.76	0.257	0.269	170.32	0.260	0.273
	4	204.59	225.27	0.270	204.34	225.59	0.269	0.283	228.05	0.270	0.284
CFCF	1	44.23	46.62	0.218	44.26	46.69	0.217	0.223	47.42	0.202	0.210
	2	54.87	58.28	0.209	54.87	58.33	0.209	0.214	58.94	0.195	0.203
	3	100.52	112.25	0.238	100.43	112.28	0.242	0.248	113.05	0.238	0.247
	4	107.56	117.43	0.249	107.46	117.61	0.250	0.258	118.44	0.249	0.261

Table 4: Undamped and damped modal frequencies and loss factors for the sandwich plate with ISD112 core.

359 The results in Tab. 4 show that the damped eigenfrequencies  $f$  and the approximate loss factors  
 360  $\eta_1$  obtained by the present SGUF-Ritz with the ADF-3 model of [19] agree very well with the  
 361 values  $(f, \eta_l)$  reported by Bilasse *et al.* [42]. The damped properties computed upon adopting the  
 362 FDZ model obtained from the ADF-5 model of [5] are also in agreement: the maximum discrepancy  
 363 attributed to the different VEM model is found to be less than 6%. It should be noted that loss factors

364 obtained at the end of the fixed-point iteration can be quite different from those estimated from the  
 365 assumption  $\omega \approx \omega_0$ . This means that care should be taken adopting a computationally less expensive  
 366 simplified approach for solving the nonlinear eigenvalue problem of frequency-dependent VEM.

367 In order to evaluate the impact of the iterative procedures, the ICE and IMSE solvers are next  
 368 compared. For this, the results of Tab. 4 obtained with the present FDZ model for the fully clamped  
 369 panel are extended to the first 50 modes. In this case, a Ritz solution of higher order is required  
 370 with  $R = S = 24$ , with a total number of DOF equal to 5184. Figure 6 (left) reports the damped  
 371 frequencies and loss factors obtained by both solvers, while Fig. 6 (right) displays the relative  
 372 percentage difference between the two solvers. The IMSE approach is seen to match well the ICE  
 373 solution, with maximum discrepancies in the loss factor and eigenfrequencies that are less than 5%  
 374 and 2%, respectively. Note that the loss factor of the VEM is larger than 1 for frequencies larger  
 375 than 300 Hz, see Fig. 1. The accuracy of IMSE comes along with a substantially less important  
 376 computational effort: for reaching the tight tolerance of  $\epsilon = 10^{-6}$  for each of the 50 modes, the ICE  
 377 requires 7 iterations, each involving a complex eigenvalue extraction, while the IMSE needs only 6  
 378 iterations involving only a real eigenproblem to be solved; the IMSE requires eventually only 60%  
 379 of the computational time required by the ICE.

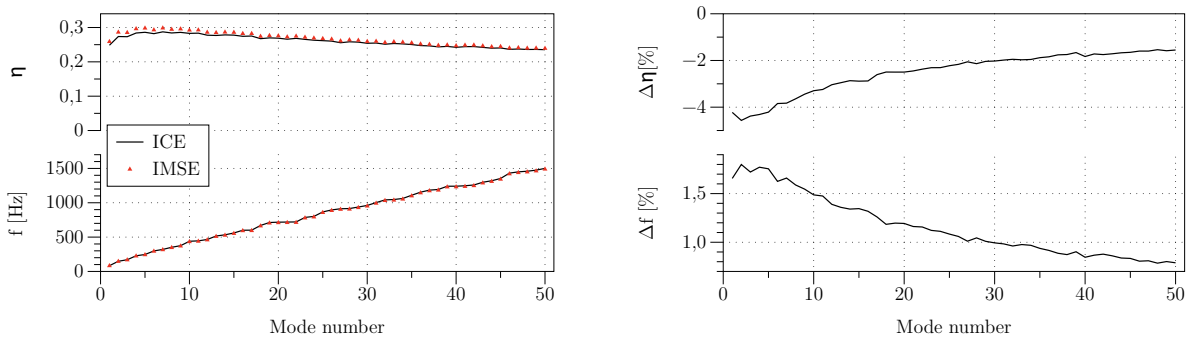


Figure 6: Sandwich plate with ISD112 core (CCCC): comparison between the ICE and IMSE solvers.

380 The damped dynamic structural response of the sandwich panel with ISD112 core is next con-  
 381 sidered. The panel is simply-supported (SSSS) and subjected to a harmonic point load excitation  
 382 of  $F = -2$  kN acting in  $P(x = L_1/4, y = L_2/4)$  over the frequency range  $f \in [0, 300]$  Hz. Figure  
 383 7 displays the FRF of the point  $P$  obtained with the FDZ model with a converged Ritz solution  
 384 ( $R = S = 14$ , thus 1764 DOF). Present results obtained with the FDZ model are compared to  
 385 those digitised from the graphics reported by Bilasse and Oguamanam [79], obtained with the same

386 ADF-3 model of [19]. Three sets of results are reported, namely the DFR and the frequency re-  
 387 sponse computed by the modal projection approach labelled “RBn”, where  $n$  indicates the number  
 388 of real and undamped modes that span the projection basis. The results pertaining to a small basis  
 389 with  $n = 5$  and a rich one with  $n = 150$  are given in Fig. 7. An overall reasonable agreement with  
 390 the solutions provided by Bilasse and Oguamanam [79] is found: the maximum discrepancies of  
 391 less than 2 [dB] are attributed to the different numerical method adopted by [79], based on FEM and  
 392 ANM. It is worthwhile noticing that the accuracy of the reduced basis approach could be improved  
 393 upon including the damping of the system, i.e., using complex modes instead of real modes, and  
 394 upon adopting a static correction [21]. As far as the computational cost is concerned, the RB5 and  
 395 RB150 take 40% and 65% of the time required for solving the DFR, respectively.

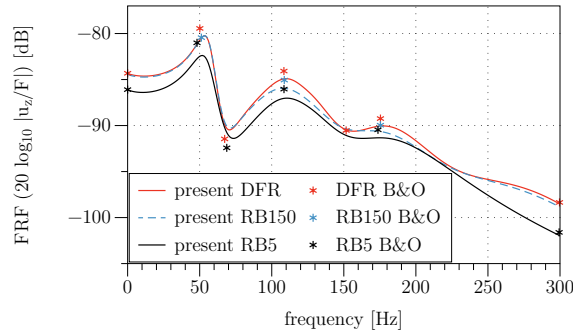


Figure 7: Frequency response function of  $P(x, y) = (L_1/4, L_2/4)$  of the SSSS sandwich plate with ISD112 core: Direct Frequency Response (DFR) and FR obtained from a real basis with 5 and 150 modes.

#### 396 4.2. Sandwich structures with multiple cores

397 The previous case studies adopted a first-order kinematics for all plies constituting the sandwich  
 398 plate, and they thus allowed to validate the proposed modelling framework based on the Ritz method  
 399 for viscoelastically damped structures. In the remainder of the paper, the attention will be given  
 400 to the variable kinematics capabilities of the SGUF upon introducing different kinematics for the  
 401 description of individual layers constituting composite plates that host multiple viscoelastic plies.

##### 402 4.2.1. Double-core sandwich beam

403 This case study has been proposed by Lewandowski and Baum [43] and examines the first  
 404 four vibration modes of a moderately thick sandwich beam of length  $L_1 = 200$  mm and thickness  
 405  $H = 11$  mm, consisting of 3 elastic plies separated by two VEM cores. The elastic and isotropic

406 plies are made out of Aluminium ( $E_f = 70.3$  GPa,  $\nu_f = 0.3$ ,  $\rho_f = 2690$  kg m<sup>-3</sup>); the outer plies  
407 have a thickness of  $h_1 = h_5 = 1$  mm and the central ply has a thickness of  $h_3 = 5$  mm. The two  
408 VEM cores have a thickness of  $h_2 = h_4 = 2$  mm each and are made out of a frequency-dependent  
409 polymer whose behaviour is described in terms of the four-parameter FDZ model according to the  
410 data reported in Tab. 5. The VEM is isotropic with a constant Poisson's coefficient  $\nu_c = 0.5$  and  
411 mass density  $\rho_c = 1600$  kg m<sup>-3</sup>. Three kinds of boundary conditions are investigated with increasing  
412 degree of static indeterminacy, namely a cantilever (clamped-free), a propped (clamped-supported)  
413 and a clamped (clamped-clamped) configuration.

$$\underline{\underline{E_0 = 1.5 \text{ MPa} \quad E_\infty = 69.95 \text{ MPa} \quad \alpha = 0.7915 \quad \tau = 1.4052 \cdot 10^{-5} \text{ s}}}$$

Table 5: Parameters of the FD Zener model for the polymer used in the double-core sandwich beam.

414 Lewandowski and Baum employed a LW model based on CLT for the elastic plies and FSDT  
415 for the VEM plies [43]. However, the moderate slenderness of the beam and the presence of a  
416 double VEM core may require refined kinematic models for grasping the damped properties of the  
417 structure and a model assessment is, hence, proposed. Figure 8 reports the damped frequencies of  
418 the cantilever, propped and clamped beams, obtained with the present Ritz approach ( $R = 10, S = 1$ )  
419 and two different LW models: LD<sub>1,0</sub>, adopts the  $\{N_{u_1}, N_{u_3}\} = \{1, 0\}$  model in each ply, while LD4 is a  
420 quasi-3D model that adopts a fourth-order approximation for all displacement components ( $N_{u_i} = 4$   
421 for  $i = 1, 2, 3$ ) in each ply. It is worth emphasising that, contrary to LD4, LD<sub>1,0</sub> employs the  
422 reduced stiffnesses in accordance with the plane stress assumption ( $N_{u_3} = 0$ ). The curves reported  
423 in Fig. 8 show an excellent agreement between these two models for the 3 boundary conditions, and  
424 an overall good agreement with the results reported by Lewandowski and Baum (L&B) [43].

425 The modal loss factors of the cantilever, propped and clamped beams, obtained by several kine-  
426 matic models, are reported in Fig. 9. In addition to the LD4 and the LD<sub>1,0</sub> models, two other  
427 models are considered which all keep the same  $\{N_{u_1}, N_{u_3}\} = \{1, 0\}$  kinematics for the elastic plies  
428 but differ in the assumptions made for the VEM core: the  $\{1, 0\}/\{3, 0\}$  model adopts a third-order  
429 expansion for the in-plane displacement ( $N_{u_1} = 3$ ) with a constant out-of-plane deflection ( $N_{u_3} = 0$ ),  
430 which calls for the use of the reduced plane stress constitutive law; the  $\{1, 0\}/\{1, 2\}$  model adopts  
431 a  $\{N_{u_1}, N_{u_3}\} = \{1, 2\}$  kinematics, which includes a linearly varying transverse normal deformation  
432 in the VEM cores and, therefore, the full 3D constitutive law. The number of parameters of the

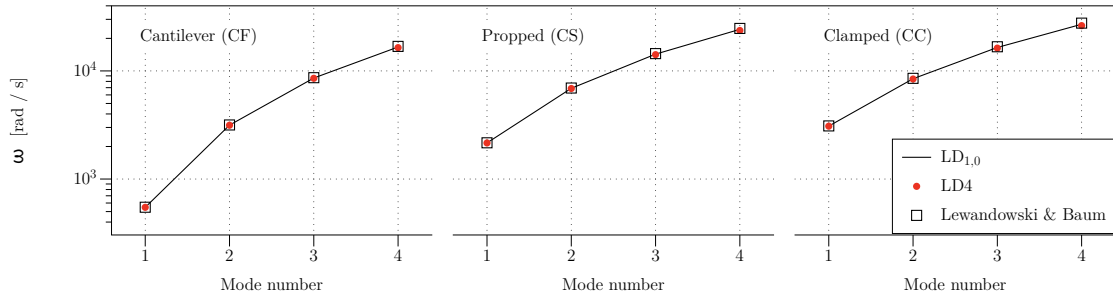


Figure 8: Double-core sandwich beam with frequency-dependent VEM: modal circular frequencies for the cantilever, propped and clamped configurations.

433 adopted structural models is 13 for  $LD_{1,0}$ , 21 for  $\{1, 0\}/\{3, 0\}$ , 17 for  $\{1, 0\}/\{1, 2\}$  and 63 for LD4.

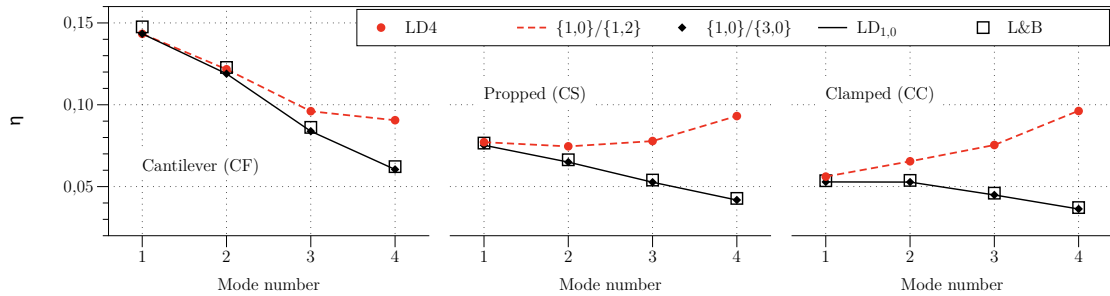


Figure 9: Double-core sandwich beam with frequency-dependent VEM: modal loss factors for the cantilever, propped and clamped configurations.

434 While the damped frequency appears to be rather insensitive to the kinematics employed in the  
 435 LW models, Fig. 9 shows a substantially different behaviour between the models retaining the full  
 436 3D constitutive law (i.e., LD4 and  $\{1, 0\}/\{1, 2\}$ ) and those relying on the plane stress assumption  
 437 (i.e., L&B,  $LD_{1,0}$  and  $\{1, 0\}/\{3, 0\}$ ). It can be seen that the transverse normal deformation enhances  
 438 the modal loss factor, this increase being more pronounced with a higher degree of hyperstaticity  
 439 and for the higher modes. On the contrary, if the transverse normal deformation within the VEM  
 440 cores is neglected, the modal loss factor appears to decrease with mode number and degree of  
 441 hyperstaticity. These results show that transverse compressional damping can play a significant role  
 442 in the modal response of sandwich structures, which thus calls for refined plate models that retain  
 443 the full 3D constitutive law.

444 4.3. Dynamic response of a triple-core panel

445 A new case study is finally proposed that deals with the dynamic characterisation of a non-  
 446 conventional, triple-core sandwich construction. The configuration is inspired from the studies for  
 447 innovative solutions for helicopter cabin noise reduction, which has been the research activity of the  
 448 Action Group 20 promoted by the *Garteur* consortium [80]. The panel is of moderate slenderness,  
 449 with a square planform with  $L_1 = L_2 = 840$  mm and a total thickness of  $H = 21.68$  mm. Figure 10  
 450 illustrates the composite stack made out of 13 plies: it consists of a symmetric layup of 4 plies of  
 451 glass fabric (GFRP) and a nomex honeycomb core glued to a melamine foam. Ply thicknesses as  
 452 well as elastic material data are reported in Tab. 6. Following the recommendations of the *Garteur*  
 453 consortium, the loss factors are considered frequency-independent.

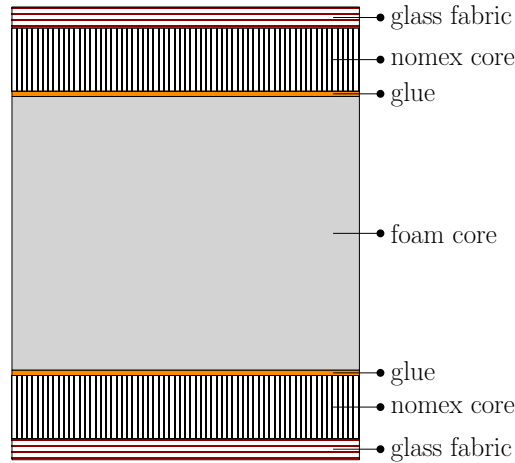


Figure 10: Sketch of triple-core sandwich stack.

Material (ply no.)	$h_p$ [mm]	$E_1 = E_2$	$E_3$	$\nu$	$G_{12}$	$G_{13}$	$G_{23}$	$\eta$ [%]	$\rho$ [ $\frac{\text{kg}}{\text{m}^3}$ ]
GFRP (1–4; 10–13)	0.275	21 000	21 000	0.13	3 000	3 000	3 000	0.01	1600
Nomex (5; 9)	3	1	330	0	1	85	38	0.05	96
Glue (6; 8)	0.240	1 950	1 950	0.4	700	700	700	0.01	1050
Melamine foam (7)	13	0.5	0.23	0	0.065	0.065	0.065	0.1	11.7

Table 6: Material data and stacking sequence of the triple-core panel (moduli expressed in [MPa]).

454 Gorgeri *et al.* investigated the free-vibration response of the fully clamped panel and compared  
 455 the numerical predictions obtained by the present Ritz-SGUF approach against experimental values  
 456 [74]. Converged solutions were obtained with Ritz expansion orders  $R = S = 26$  and these orders

457 are employed for the present analysis as well. The first 300 natural frequencies of the panel are  
 458 reported in Fig. 11 for 3 different kinematic models for the melamine foam core, labelled in the  
 459 following as  $\text{MF}\{N_{u_\alpha}, N_{u_3}\}$ : the  $\text{MF}\{1,0\}$  model adopts the FSDT kinematics and the reduced consti-  
 460 tutive law, while the  $\text{MF}\{3,2\}$  and the  $\text{MF}\{1,2\}$  models retain the 3D constitutive law. The other plies  
 461 are modelled as follows: the 4 GFRP plies are regrouped in 1 sublaminates with FSDT kinematics;  
 462 the nomex core and glue ply form another sublaminates, for which a ply-wise FSDT model has been  
 463 adopted. As a result, the SGUF models adopting the  $\{3, 2\}$ , the  $\{1, 2\}$  and the  $\{1, 0\}$  kinematics for  
 464 the melamine foam ply have 23, 19 and 17 parameters, respectively, and their corresponding total  
 465 DOF number are thus 15 548, 12 844 and 11 492, respectively. A shear correction factor of  $\kappa^2 = 5/6$   
 466 has been employed for the FSDT and  $\{1, 2\}$  kinematics.

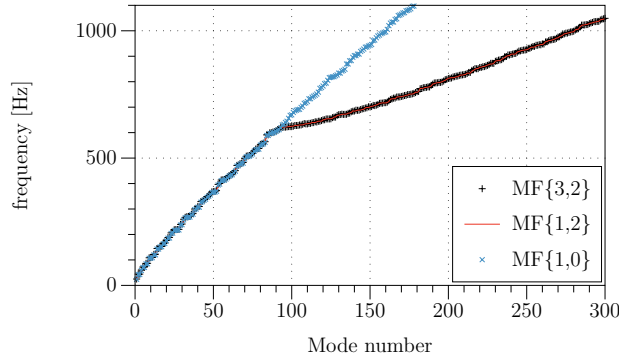


Figure 11: First 300 natural frequencies of the CCCC triple-core panel for 3 models for the melamine foam core.

467 The analysis in [74] showed that vibration modes with eigenfrequencies higher than 620 Hz  
 468 started to involve important through-the-thickness stretch of the weak melamine foam core. This  
 469 transition is characterised in Fig. 11 by an abrupt change of slope of the curve: the modal density  
 470 is higher for  $f > 620$  Hz, due to the presence of both long-wave thickness modes and in-plane  
 471 modes with decreasing wavelengths. Figure 12 illustrates exemplarily 4 couples of modal shapes  
 472 in terms of in-plane patterns and cross-sectional views, where each couple shares the same number  
 473 of half-waves along the in-plane directions  $x$  and  $y$ . The first couple Fig. 12(a) and Fig. 12(b) has  
 474 one half-wave in the  $(x, y)$ -plane and concerns the modes number 1 (25.0 Hz) and 94 (621.0 Hz); it  
 475 is noted that the latter mode has a predominant through-the-thickness deformation of the melamine  
 476 foam core. The subsequent modes 95, 97 and 98, reported in Fig. 12(d), Fig. 12(f) and Fig. 12(h),  
 477 respectively, occur within a narrow frequency band beyond 621 Hz: these are again essentially  
 478 thickness-stretch modes whose in-plane pattern is defined by a rather low number of half-waves,



479 just as the modes 2,4 and 5 reported in Fig. 12(c), Fig. 12(e) and Fig. 12(g), respectively.

480 From Fig. 11 it is evident that if FSDT kinematics is adopted for the melamine foam, then no  
 481 change in the modal density occurs because no thickness modes can be captured. Furthermore, the  
 482 results of MF{3,2} and MF{1,2} are barely distinguishable, a third-order shear deformation is thus  
 483 not as relevant as the inclusion of the thickness stretch. Results obtained with refined kinematic  
 484 models for the nomex cores have been omitted for the sake of brevity because no relevant difference  
 485 has been found in the considered frequency range.

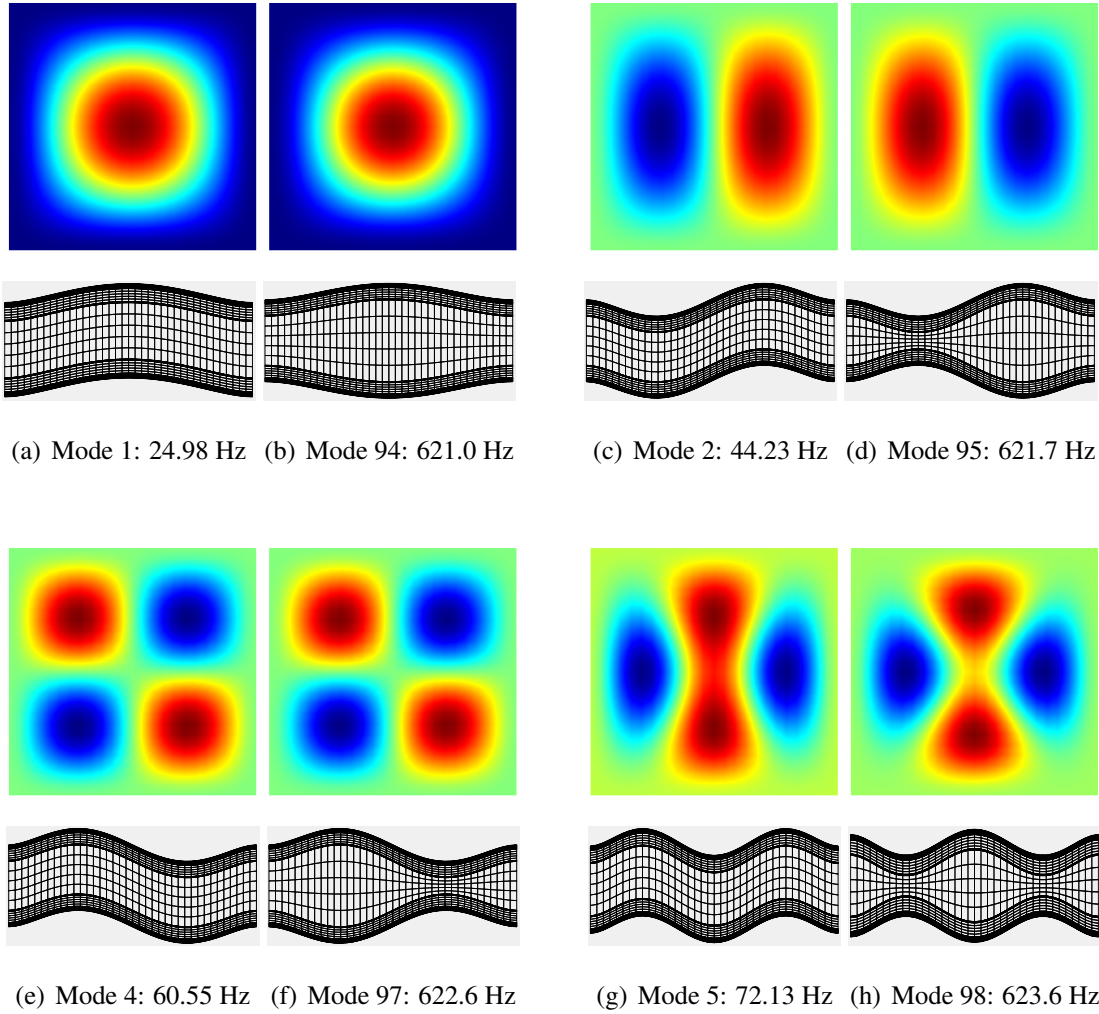


Figure 12: Modal shapes with similar in-plane pattern but different through-the-thickness deformation.

486 In the following, the focus is set on the frequency response over the range  $f \in [0, 600]$  Hz of  
 487 the fully clamped panel excited at  $P(x_1 = \frac{L_1}{4}, x_2 = \frac{L_2}{4}, z = \frac{h}{2})$  by a harmonic force of magnitude  
 488  $F = -2$  kN. The DFR of point  $P$  obtained with the MF{1,2} and MF{1,0} models is given in Fig. 13  
 489 (left). A good agreement is found for  $f \leq 300$  Hz: the MF{1,0} model captures well all peaks, except

490 for the response at  $f \approx 150$  Hz, where it predicts a lower amplitude compared to the MF{1,2} model.  
 491 The discrepancies increase for higher frequencies, where MF{1,0} systematically underestimates the  
 492 response. From the amplitude and phase plots corresponding to the FRF, shown in Fig. 13 (right), it  
 493 appears that the main discrepancies arise in the phase diagram, i.e., due to a different representation  
 494 of the viscoelastic damping of the melamine foam. One may notice the large differences at  $f \approx$   
 495 150 Hz as well as for  $f > 300$  Hz.

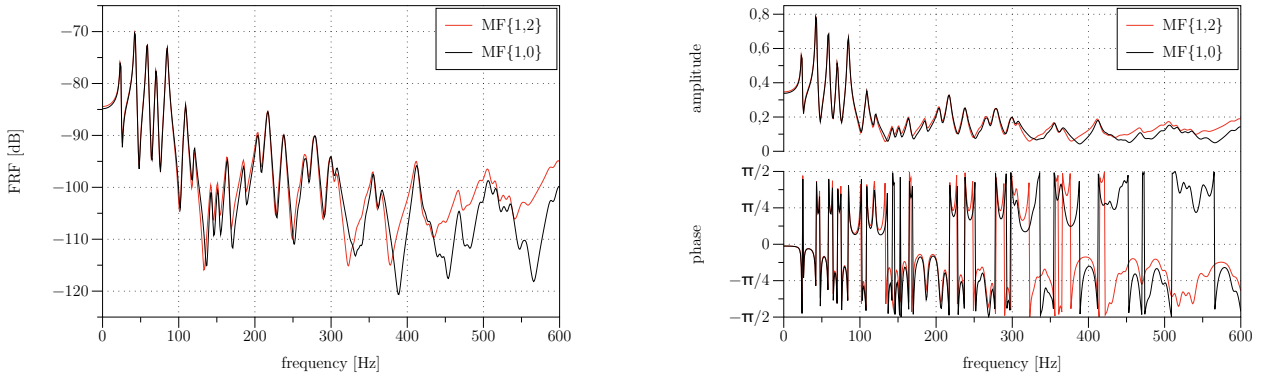


Figure 13: FRF of the triple-core panel (left) and related amplitude and phase diagrams (right): comparison of MF{1,2} and MF{1,0} models.

496 The DFR is next compared against the FRF obtained by means of the projection on the first  $n$   
 497 real undamped modes, with  $n = \{25, 50, 100, 150\}$ , see Fig. 14. From the free-vibration analysis  
 498 results in Fig. 11, the eigenfrequencies  $f_n$  of the  $n^{\text{th}}$  mode are  $f_{25} = 216.1$  Hz,  $f_{50} = 365.8$  Hz,  
 499  $f_{100} = 625.3$  Hz,  $f_{150} = 701.2$  Hz. The FRF spanned by the first 25 and 50 real modes are obviously  
 500 limited to the corresponding maximum frequencies. A good agreement is however found for the  
 501 low frequency range  $f \leq 110$  Hz, i.e., half of the maximum frequency retained in the RB25. The  
 502 RB100 and RB150 solutions yield similar FRF, with a slight accuracy increase of the RB150 in the  
 503 high frequency range  $f > 300$  Hz. In this region, it is further noticed that the differences between  
 504 the RB100 and RB150 are smaller if the MF{1,0} model is used for the weak and highly damping  
 505 melamine foam ply. The discrepancies of the modal projection solutions with respect to the DFR  
 506 are generally larger if the MF{1,2} model is used. This is attributed to the need of the truncated basis  
 507 to include several thickness modes in order to represent the damping effect of the melamine foam.

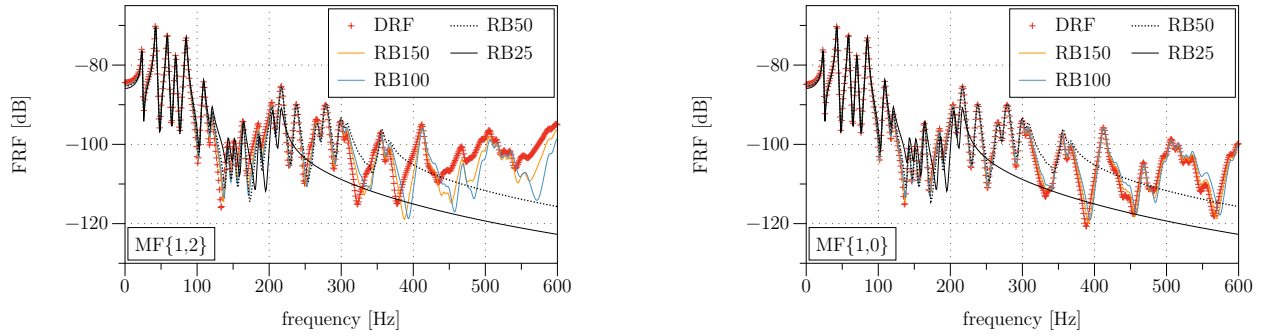


Figure 14: FRF of the triple-core panel obtained by DFR and by  $RB_n$  modal projection: MF{1,2} model (left) and MF{1,0} model (right).

## 508 5. Conclusions

509 The paper discussed the extension of the SGUF-Ritz formulation to the dynamic response in the  
510 frequency domain of composite panels hosting viscoelastic plies. Due to the primary role played by  
511 sandwich structures in many mechanical and aerospace applications, this extension represents an  
512 important step toward the development of a numerical tool capable to analyse more realistic panel  
513 configurations, including viscoelastic layers for vibration or acoustic damping. The approach is  
514 developed in the framework of the variable kinematics SGUF formulation, and approximate solu-  
515 tions are retrieved by referring to an efficient Ritz method. The main advantage of the proposed  
516 strategy relies in the possibility of modelling any configuration with the desired level of detail by  
517 properly combining the definition of the sublaminates with the corresponding kinematic theories.  
518 Therefore, the structural model for sandwich panels can be tuned to the desired accuracy upon in-  
519 troducing dedicated assumptions for the behaviour of the stiff skins and the soft cores. In fact,  
520 classical models with few parameters and refined models requiring a larger number of parameters  
521 can be combined, in order to achieve a best compromise between accuracy and number of degrees  
522 of freedom, i.e., for optimising the computational efficiency. Moreover, the influence of specific  
523 model assumptions can be assessed in a straightforward manner, as exemplarily highlighted with  
524 respect to the  $\sigma_{zz} = 0$  assumption in VEM cores. Special attention has been paid to the description  
525 of the frequency-dependent viscoelastic behaviour, for which a fractional derivatives Zener-type  
526 model has been implemented along with more conventional models relying on series expansions.  
527 Different solution procedures for the complex eigenvalue problem have been also prototypically im-  
528 plemented. The quality of the predictions is demonstrated by comparison with available solutions

529 for different panels, demonstrating that quasi-3D accuracy can be achieved with a relatively small  
530 number of degrees of freedom, much less with respect to those required by a purely LW approach.  
531 Conventional single-core sandwich plates as well complex multi-core panels can be investigated,  
532 irrespective of the thickness and of the boundary conditions.

533 Further work shall address the extension to curved panels, the evaluation of acoustic properties  
534 and the optimisation of viscoelastic composite panels. In order to quantitatively assess the accuracy  
535 and, hence, the efficiency of the various structural kinematics, it could be useful to introduce an  
536 error measure accounting for the strain and kinetic energy contributions that define the dynamic  
537 response of the sandwich panel. The computational efficiency of the approach could be also further  
538 improved upon adopting enhanced reduced-order modelling techniques. Finally, it is worthwhile  
539 mentioning that the modal response or the direct FRF obtained by efficient computational tools like  
540 the present one could be advantageously used within inverse identification techniques for character-  
541 ising the frequency-dependent damping properties of the sandwich plate; this would allow to take  
542 into account the alteration of the bare VEM properties induced by the process for manufacturing  
543 the composite structure.

#### 544 **Acknowledgments**

545 Riccardo Vescovini and Lorenzo Dozio would like to thank Ministero dell'Istruzione, dell'Università  
546 e della Ricerca for funding this research under PRIN 2017 program.

---

**Algorithm 1** The ICE algorithm for  $N$  modes

---

- 1: solve Eq. (18) with  $\omega = 0$ : compute  $\lambda(0)$  ▷ Initial guess:  $N$  real eigenvalues
  - 2: **for**  $j = 1 : N$  **do**
  - 3:     Initialise the error  $\epsilon = 1$  and the eigenfrequency  $\tilde{\omega} = \lambda_j(0)$
  - 4:     **while**  $\epsilon > \epsilon_{tol}$  **do** ▷ used tolerance:  $\epsilon_{tol} = 1e^{-6}$
  - 5:         solve  $[\mathbf{K}^*(\tilde{\omega}) - \lambda^2(\tilde{\omega})\mathbf{M}]U = \mathbf{0}$
  - 6:         compute the error:  $\epsilon = \frac{\tilde{\omega} - \sqrt{\text{Re}(\lambda_j^2(\tilde{\omega}))}}{\sqrt{\text{Re}(\lambda_j^2(\tilde{\omega}))}}$
  - 7:         update the eigenfrequency:  $\tilde{\omega} = \sqrt{\text{Re}(\lambda_j^2(\tilde{\omega}))}$
  - 8:     **end while**
  - 9:      $\omega_j = \tilde{\omega}$ ;  $\eta_j = \frac{\text{Im}(\lambda_j^2)}{\text{Re}(\lambda_j^2)}$  ▷ converged solution: damped eigenfrequencies & modal loss factor
  - 10: **end for**
- 

---

**Algorithm 2** The IMSE algorithm for  $N$  modes

---

- 1: solve Eq. (18) with  $\omega = 0$ : compute  $\lambda(0)$  ▷ Initial guess:  $N$  real eigenvalues
  - 2: **for**  $j = 1 : N$  **do**
  - 3:     Initialise the error  $\epsilon = 1$  and the eigenfrequency  $\tilde{\omega} = \lambda_j(0)$
  - 4:     **while**  $\epsilon > \epsilon_{tol}$  **do** ▷ used tolerance:  $\epsilon_{tol} = 1e^{-6}$
  - 5:         solve  $[\text{Re}(\mathbf{K}^*(\tilde{\omega})) - \lambda^2(\tilde{\omega})\mathbf{M}]U = \mathbf{0}$
  - 6:         compute the error:  $\epsilon = \frac{\tilde{\omega} - \lambda_j(\tilde{\omega})}{\lambda_j(\tilde{\omega})}$
  - 7:         update the eigenfrequency and modal shapes:  $\tilde{\omega} = \lambda_j(\tilde{\omega})$ ;  $\mathbf{U}_j = \mathbf{U}_j(\tilde{\omega})$
  - 8:     **end while**
  - 9:      $\omega_j = \tilde{\omega}$ ;  $\eta_j = \frac{\mathbf{U}_j^T \text{Im}(\mathbf{K}(\omega_j)) \mathbf{U}_j}{\mathbf{U}_j^T \text{Re}(\mathbf{K}(\omega_j)) \mathbf{U}_j}$  ▷ converged solution: damped eigenfrequencies & modal loss factor
  - 10: **end for**
-

548 **References**

- 549 [1] M. D. Rao, Recent applications of viscoelastic damping for noise control in automobiles and  
550 commercial airplanes, *J. Sound Vibr.* 262 (2003) 457–474.
- 551 [2] A. M. Baz, *Active and Passive Vibration Damping*, John Wiley & Sons, Ltd, 2019.
- 552 [3] D. I. G. Jones, On the temperature-frequency analysis of polymer dynamic mechanical be-  
553 haviour, *J. Sound Vibr.* 140 (1990) 85–102.
- 554 [4] D. J. McTavish, P. C. Hughes, Modeling of linear viscoelastic space structures, *J. Vibr. Acoust.*  
555 115 (1993) 103–110.
- 556 [5] G. A. Lesieutre, E. Bianchini, Time domain modeling of linear viscoelasticity using anelastic  
557 displacement fields, *J. Vibr. Acoust.* 117 (1995) 424–430.
- 558 [6] R. L. Bagley, P. J. Torvik, A theoretical basis of the application of fractional calculus to vis-  
559 coelasticity, *J. Rheol.* 27 (3) (1983) 201–210.
- 560 [7] R. Koeller, Applications of fractional calculus to the theory of viscoelasticity, *J. Appl. Mech.*  
561 51 (12) (1984) 299–307.
- 562 [8] R. L. Bagley, P. J. Torvik, On the fractional calculus model of viscoelastic behavior, *J. Rheol.*  
563 30 (3) (1986) 133–155.
- 564 [9] T. Pritz, Analysis of four-parameter fractional derivative model of real solid materials, *J. Sound*  
565 *Vibr.* 195 (1996) 103–115.
- 566 [10] T. Pritz, Five-parameter fractional derivative model for polymeric damping materials, *J. Sound*  
567 *Vibr.* 265 (2003) 935–952.
- 568 [11] A. C. Galucio, J.-F. Deü, R. Ohayon, Finite element formulation of viscoelastic sandwich  
569 beams using fractional derivative operators, *Comput. Mech.* 33 (2004) 282–291.
- 570 [12] H. Voss, An Arnoldi method for nonlinear eigenvalue problems, *BIT Numer. Math.* 44 (2004)  
571 387–401.
- 572 [13] X. Chen, H. L. Chen, X. L. Hu, Damping predication of sandwich structures by order-  
573 reduction-iteration approach, *J. Sound Vibr.* 222 (1999) 803–812.

- 574 [14] B.-A. Ma, J.-F. He, A finite element analysis of viscoelastically damped sandwich plates,  
575 J. Sound Vibr. 152 (1992) 107–123.
- 576 [15] E. M. Daya, M. Potier-Ferry, A numerical method for nonlinear eigenvalue problems applica-  
577 tion to vibrations of viscoelastic structures, Comput. Struct. 79 (2001) 533–541.
- 578 [16] M. L. Soni, Finite element analysis of viscoelastically damped sandwich structures, in: The  
579 Shock and Vibration Bulletin, Vol. 51 (Pt 1), The Shock and Vibration Information Center,  
580 1981, pp. 97–109.
- 581 [17] E. E. Ungar, E. M. Kerwin, Jr., Loss factors of viscoelastic systems in terms of energy con-  
582 cepts, J. Acoust. Soc. Am. 34 (7) (1962) 954–957.
- 583 [18] C. D. Johnson, D. A. Kienholz, Finite element prediction of damping in structures with con-  
584 strained viscoelastic layers, AIAA J. 20 (1982) 1284–1290.
- 585 [19] M. A. Trindade, A. Benjeddou, R. Ohayon, Modeling of frequency-dependent viscoelastic  
586 materials for active-passive vibration damping, J. Vibr. Acoust. 122 (2000) 169–174.
- 587 [20] R. A. S. Moreira, J. Dias Rodrigues, Multilayer damping treatments: modeling and experi-  
588 mental assessment, J. Sandwich Struct. Mater. 12 (2010) 181–198.
- 589 [21] L. Rouleau, J.-F. Deü, A. Legay, A comparison of model reduction techniques based on modal  
590 projection for structures with frequency-dependent damping, Mech. Syst. Signal Pr. 90 (2017)  
591 110–125.
- 592 [22] E. M. Kerwin, Jr., Damping of flexural waves by a constrained viscoelastic layer,  
593 J. Acoust. Soc. Am. 31 (7) (1959) 952–962.
- 594 [23] B. E. Douglas, J. C. S. Yang, Transverse compressional damping in the vibratory response of  
595 elastic-viscoelastic-elastic beams, AIAA J. 16 (1978) 925–930.
- 596 [24] C. M. A. Vasques, L. C. Cardoso, Viscoelastic damping technologies: Finite element model-  
597 ing and application to circular saw blades, in: C. M. A. Vasques, J. Dias Rodrigues (Eds.),  
598 Vibration and Structural Acoustics Analysis, Springer Science+Business Media B. V., 2011,  
599 Ch. 9, pp. 207–264.

- 600 [25] L. Rouleau, A. Legay, J.-F. Deü, Interface finite elements for the modelling of constrained  
601 viscoelastic layers, *Compos. Struct.* 204 (2018) 847–854.
- 602 [26] F. Kpeky, H. Boudaoud, F. Abed-Meraim, E. M. Daya, Modeling of viscoelastic sandwich  
603 beams using solid–shell finite elements, *Compos. Struct.* 133 (2015) 105–116.
- 604 [27] E. Carrera, Theories and finite elements for multilayered, anisotropic, composite plates and  
605 shells, *Arch. Comput. Meth. Eng.* 9 (2002) 87–140.
- 606 [28] J. N. Reddy, *Mechanics of Laminated Composite Plates and Shells: Theory and Analysis*, 2nd  
607 Edition, CRC Press, 2004.
- 608 [29] M. D’Ottavio, O. Polit, Classical, first order, and advanced theories, in: H. Abramovich (Ed.),  
609 *Stability and Vibration of Thin-Walled Composite Structures*, *Composites Science and Engi-*  
610 *neering*, Woodhead Publishing, 2017, Ch. 3, pp. 91–140.
- 611 [30] E. Carrera, Historical review of zig-zag theories for multilayered plates and shells,  
612 *Appl. Mech. Rev.* 56 (2003) 287–308.
- 613 [31] A. Loredo, M. D’Ottavio, P. Vidal, O. Polit, A family of of higher-order single layer plate  
614 models meeting  $C_z^0$ -requirements for arbitrary laminates, *Compos. Struct.* 225 (2019) 111146.
- 615 [32] R. M. J. Groh and P. M. Weaver, On displacement-based and mixed-variational equivalent  
616 single layer theories for modelling highly heterogeneous laminated beams, *Int. J. Solids Struct.*  
617 59 (2015) 147–170.
- 618 [33] H. Hu, S. Belouettar, M. Potier-Ferry, E. M. Daya, Review and assessment of various theories  
619 for modeling sandwich composites, *Compos. Struct.* 84 (2008) 282–292.
- 620 [34] E. Carrera, S. Brischetto, A survey with numerical assessment of classical and refined theories  
621 for the analysis of sandwich plates, *Appl. Mech. Rev.* 62 (2009) 1–17.
- 622 [35] R. A. DiTaranto, Theory of vibratory bending for elastic and viscoelastic layered finite-length  
623 beams, *J. Appl. Mech.* 32 (1965) 881–886.
- 624 [36] D. J. Mead, S. Markus, The forced vibration of a three-layer, damped sandwich beam with  
625 arbitrary boundary conditions, *J. Sound Vibr.* 10 (1969) 163–175.



- 626 [37] J.-F. He, B.-A. Ma, Analysis of flexural vibration of viscoelastically damped sandwich plates,  
627 J. Sound Vibr. 126 (1988) 37–47.
- 628 [38] Q. J. Zhang, M. G. Sainsbury, The Galerkin element method applied to the vibration of rect-  
629 angular damped sandwich plates, Comput. Struct. 74 (2000) 717–730.
- 630 [39] A. Fasana, S. Marchesiello, Rayleigh-Ritz analysis of sandwich beams, J. Sound Vibr. 241  
631 (2001) 643–652.
- 632 [40] M. D. Rao, S. He, Dynamic analysis and design of laminated composite beams with multiple  
633 damping layers, AIAA J. 31 (1993) 736–745.
- 634 [41] J. S. Moita, A. L. Araújo, P. Martins, C. M. Mota Soares, C. A. Mota Soares, A finite element  
635 model for the analysis of viscoelastic sandwich structures, Comput. Struct. 89 (2011) 1874–  
636 1881.
- 637 [42] M. Bilasse, L. Azrar, E. M. Daya, Complex modes based numerical analysis of viscoelastic  
638 sandwich plates vibrations, Comput. Struct. 89 (2011) 539–555.
- 639 [43] R. Lewandowski, M. Baum, Dynamic characteristics of multilayered beams with viscoelastic  
640 layers described by the fractional Zener model, Arch. Appl. Mech. 85 (2015) 1793–1814.
- 641 [44] K. Akoussan, H. Boudaoud, E. M. Daya, Y. Koutsawa, E. Carrera, Sensitivity analysis of the  
642 damping properties of viscoelastic composite structures according to the layers thicknesses,  
643 Compos. Struct. 149 (2016) 11–25.
- 644 [45] W. Larbi, J.-F. Deü, R. Ohayon, Vibroacoustic analysis of double-wall sandwich panels with  
645 viscoelastic core, Comput. Struct. 174 (2016) 92–103.
- 646 [46] S. Ren, G. Zhao, A four-node quadrilateral element for vibration and damping analysis of  
647 sandwich plates with viscoelastic core, J. Sandwich Struct. Mater. 21 (2019) 1072–1118.
- 648 [47] P. Cupiał, J. Nizioł, Vibration and damping analysis of a three-layered composite plate with  
649 viscoelastic mid-layer, J. Sound Vibr. 183 (1995) 99–114.
- 650 [48] R. Rikards, A. Chate, E. Barkanov, Finite element analysis of damping the vibrations of lami-  
651 nated composites, Comput. Struct. 47 (1993) 1005–1015.

- 652 [49] R. A. S. Moreira, J. Dias Rodrigues, A. J. M. Ferreira, A generalized layerwise finite element  
653 for multi-layer damping treatments, *Comput. Mech.* 37 (2006) 426–444.
- 654 [50] Z. Huang, Z. Qin, F. Chu, Vibration and damping characteristics of sandwich plates with  
655 viscoelastic core, *J. Vibr. Control* 22 (2016) 1876–1888.
- 656 [51] A. L. Araújo, C. M. Mota Soares, C. A. Mota Soares, J. Herskovits, Optimal design and pa-  
657 rameter estimation of frequency dependent viscoelastic laminated sandwich composite plates,  
658 *Compos. Struct.* 92 (2010) 2321–2327.
- 659 [52] J. S. Moita, A. L. Araújo, C. M. Mota Soares, C. A. Mota Soares, Finite element model for  
660 damping optimization of viscoelastic sandwich structures, *Adv. Eng. Software* 66 (2013) 34–  
661 39.
- 662 [53] T. S. Plagianakos, D. A. Saravanos, High-order layerwise finite element for the damped  
663 free-vibration response of thick composite and sandwich composite plates, *Int. J. Nu-  
664 mer. Meth. Eng.* 77 (2009) 1593–1626.
- 665 [54] A. Bhimaraddi, Sandwich beam theory and the analysis of constrained layer damping, *J. Sound  
666 Vibr.* 179 (1995) 591–602.
- 667 [55] M. Ganapathi, B. P. Patel, P. Boisse, O. Polit, Flexural loss factors of sandwich and laminated  
668 composite beams using linear and nonlinear dynamic analysis, *Compos. B* 30 (1999) 245–256.
- 669 [56] A. Treviso, D. Mundo, M. Tournour, A  $C^0$ -continuous RZT beam element for the damped  
670 response of laminated structures, *Compos. Struct.* 131 (2015) 987–994.
- 671 [57] J.-W. Han, J.-S. Kim, M. Cho, Improved finite element viscoelastic analysis of laminated  
672 structures via the enhanced first-order shear deformation theory, *Compos. Struct.* 180 (2017)  
673 360–377.
- 674 [58] A. Castel, A. Loredó, A. El Hafidi, B. Martin, Complex power distribution analysis in plates  
675 covered with passive constrained layer damping patches, *J. Sound Vibr.* 331 (2012) 2485–  
676 2498.

- 677 [59] Z. Xie, W. S. Shepard, Jr, Analytical modeling and analysis of a constrained layer  
678 damped plate to examine the impact of the transverse compressional damping component,  
679 *Mech. Adv. Mater. Struct.* 21 (2014) 669–679.
- 680 [60] S. Ren, G. Zhao, S. Zhang, A layerwise finite element formulation for vibration and damping  
681 analysis of sandwich plate with moderately thick viscoelastic core, *Mech. Adv. Mater. Struct.*  
682 (2019). DOI: 10.1080/15376494.2018.1504360.
- 683 [61] M. Cinefra, E. Carrera, A. Lamberti, M. Petrolo, Best theory diagrams for multilayered plates  
684 considering multifield analysis, *J. Intellig. Mat. Sys. Struct.* 28 (2017) 2184–2205.
- 685 [62] E. Carrera, M. Cinefra, M. Petrolo, E. Zappino, *Finite Element Analysis of Structures through  
686 Unified Formulation*, John Wiley & Sons, Ltd, Chichester, UK, 2014.
- 687 [63] L. Demasi, Partially Layer Wise advanced Zig Zag and HSDT models based on the General-  
688 ized Unified Formulation, *Eng. Struct.* 53 (2013) 63–91.
- 689 [64] M. D’Ottavio, A Sublaminar Generalized Unified Formulation for the analysis of composite  
690 structures and its application to sandwich plates bending, *Compos. Struct.* 142 (2016) 187–  
691 199.
- 692 [65] A. J. M. Ferreira, A. L. Araújo, A. M. A. Neves, J. D. Rodrigues, E. Carrera, M. Cinefra,  
693 C. M. Mota Soares, A finite element model using a unified formulation for the analysis of  
694 viscoelastic sandwich laminates, *Compos. B* 45 (2013) 1258–1264.
- 695 [66] B. Liu, L. Zhao, A. J. M. Ferreira, Y. F. Xing, A. M. A. Neves, J. Wang, Analysis of viscoelastic  
696 sandwich laminates using a unified formulation and a differential quadrature hierarchical finite  
697 element method, *Compos. B* 110 (2017) 185–192.
- 698 [67] M. Filippi, E. Carrera, Various refined theories applied to damped viscoelastic beams and  
699 circular rings, *Acta Mech.* 228 (2017) 4235–4248.
- 700 [68] M. Filippi, E. Carrera, S. Valvano, Analysis of multilayered structures embedding viscoelastic  
701 layers by higher-order, and zig-zag plate elements, *Compos. B* 154 (2018) 77–89.
- 702 [69] A. Alaimo, C. Orlando, S. Valvano, Analytical frequency response solution for composite  
703 plates embedding viscoelastic layers, *Aero. Sci. Tech.* 92 (2019) 429–445.

- 704 [70] L. Dozio, E. Carrera, Ritz analysis of vibrating rectangular and skew multilayered plates based  
705 on advanced variable-kinematics models, *Compos. Struct.* 94 (2012) 2118–2128.
- 706 [71] M. D’Ottavio, L. Dozio, R. Vescovini, O. Polit, Bending analysis of composite laminated and  
707 sandwich structures using sublaminated variable-kinematic Ritz models, *Compos. Struct.* 155  
708 (2016) 45–62.
- 709 [72] R. Vescovini, M. D’Ottavio, L. Dozio, O. Polit, Buckling and wrinkling of anisotropic sand-  
710 wich plates, *Int. J. Engng. Sci.* 130 (2018) 136–156.
- 711 [73] M. D’Ottavio, L. Dozio, R. Vescovini, O. Polit, The Ritz – Sublaminated Generalized Unified  
712 Formulation approach for piezoelectric composite plates, *Int. J. Smart Nano Mater.* 9 (2018)  
713 1–22.
- 714 [74] A. Gorgeri, R. Vescovini, L. Dozio, Analysis of multiple-core sandwich cylindrical shells  
715 using a sublaminated formulation, *Compos. Struct.* 225 (2019) 111067.
- 716 [75] R. Vescovini, L. Dozio, M. D’Ottavio, O. Polit, On the application of the Ritz method to  
717 free vibration and buckling analysis of highly anisotropic plates, *Compos. Struct.* 192 (2018)  
718 460–474.
- 719 [76] L. Rouleau, Modélisation vibro-acoustique de structures sandwich munies de matériaux visco-  
720 élastiques [*Vibro-acoustic modeling of sandwich structures with viscoelastic materials*], Ph.D.  
721 thesis, Conservatoire National des Arts et Métiers (2013).  
722 URL <https://tel.archives-ouvertes.fr/tel-00957457>
- 723 [77] L. Rouleau, J.-F. Deü, A. Legay, J.-F. Sigrist, P. Marin-Courtoud, Reduced order model for  
724 noise and vibration attenuation of water immersed viscoelastic sandwich structures, in: *Pro-  
725 ceedings of Acoustics2012, Nantes, France, 2012*, pp. 733–738.
- 726 [78] J. Kennedy, R. Eberhart, Particle swarm optimization, in: *Proceedings of ICNN’95 – Interna-  
727 tional Conference on Neural Networks, Vol. 4, IEEE, 1995*, pp. 1942–1948.
- 728 [79] M. Bilasse, D. C. D. Oguamanam, Forced harmonic response of sandwich plates with vis-  
729 coelastic core using reduced-order model, *Compos. Struct.* 105 (2013) 311–318.

730 [80] F. Simon, T. Haase, O. Unruh, G. Ghiringhelli, A. Parrinello, R. Vescovini, Benchmark for  
731 modelization of acoustic transmission loss applied to helicopter trim panels, in: 42nd Euro-  
732 pean Rotorcraft Forum (ERF 2016), Lille, France, 2016.